$[^{16}O(0_2^+)+\alpha]$ parentage of continuum levels in ^{20}Ne

C. M. Laymon,* K. D. Brown,† and D. P. Balamuth
Department of Physics, University of Pennsylvania, Philadelphia, Pennsylvania 19104
(Received 23 September 1991)

A search for continuum levels in ^{20}Ne with a large $[^{16}O(0_2^+)+\alpha]$ parentage has been conducted using both resonant and direct production processes. The differential cross section for the $^{16}O(\alpha,\alpha_1)^{16}O^*(0_2^+)$ reaction has been measured at 13 to 26 angles for bombarding energies from $E_\alpha = 10.2$ to 18 MeV, mostly in 25 keV steps. Events leading to the first excited state in ^{16}O were identified by requiring the coincident observation of an α particle and an electron or positron from the internal pair decay of the ^{16}O first excited state. Amplitudes of individual partial waves were extracted from the data by parametrizing the angular distributions in terms of the complex zeros of the scattering amplitudes. An R-matrix analysis of the data reveals a $J^\pi = 2^+$ level at $E_x = 13.1$ MeV with a spectroscopic factor $\Theta^2_{\alpha_1} > 63\%$. Several individual levels, a region of overlapping $J^\pi = 4^+$ levels from $E_x = 13.69$ to 14.93 MeV and a region of $J^\pi = 6^+$ levels from $E_x = 16.73$ to 18.73 MeV, have also been analyzed in detail. Branching ratios of ^{20}Ne levels to the first excited state in ^{16}O have been measured by populating the levels with the reaction $^{12}C(^{12}C,\alpha)^{20}Ne^*$ and observing their subsequent α decay to the 0_2^+ state of ^{16}O. A $J^\pi = 6^+$ level at $E_x = 15.16$ MeV and a $J^\pi = 8^+$ level at $E_x = 18.54$ MeV, which had previously been suggested as members of a rotational band based on the $J^\pi = 0^+$ level in ^{20}Ne at $E_x = 12.44$ MeV are shown to have small values of $\Theta^2_{\alpha_1}$, arguing against this identification.

PACS number(s): 25.55.Ci, 21.10.Jx, 27.30.+t

I. INTRODUCTION

The structure of light *s-d* shell nuclei has been a particularly fruitful meeting ground for many different types of theoretical description. These range from independent particle models such as the shell model to macroscopic models that often contain a collective quadrupole degree of freedom. These two pictures have a great deal in common as can be seen from the application of SU(3) symmetry as a systematic method of basis truncation in the shell model [1]. For low-lying levels, where the number of degrees of freedom is relatively small, many of the available theoretical pictures converge: The ground-state rotational band in ^{20}Ne, for example, has been successfully described in terms of the shell model [2,3], collective model [4], and the cluster model [5,6].

In an attempt to differentiate among these various pictures and to ascertain their limitations, it is useful to probe higher regions of excitation energy where more degrees of freedom are available. It is well known that even in light systems the shell model with a tractable set of basis states cannot account for even the gross features observed. One such feature is the tendency towards cluster formation, often involving four nucleons. The description of nuclear structure in terms of α-particle-like excitations is well known [7]. From the point of view of cluster models, excitations which can be described in terms of more than two clusters are an interesting next step. In ^{20}Ne, for example, one might study 8p-4h (eight-particle–four-hole) excitations relative to a closed $1p$ shell; in the language of the cluster model, such states include excitations which can be described as two α-like clusters coupled to a ^{12}C core. Previous studies have identified candidates for such states. The $K^\pi = 0_3^+$ band starting with the level at $E_x = 7.2$ MeV is now widely believed to have predominantly such an 8p-4h structure. This conclusion was reached after a great deal of experimental work using transfer reactions. In the $^{12}C(^{12}C,\alpha)^{20}Ne$ [8,9,10] and $^{12}C(^{14}N,^6Li)^{20}Ne$ [11] reactions, eight nucleons were transferred from the projectile to the ^{12}C target. Generally levels which are now assigned to the $K^\pi = 0_3^+$ rotational band were found to be strongly excited by these reactions. This piece of spectroscopic information is, by itself, insufficient to make the assignment. The transfer of eight particles to ^{12}C could excite levels with less than four holes in the p shell, for example, 4p-0h states. Some possibilities were eliminated by carrying out other transfer reactions that start with a target with more of the p shell filled. For example, in the reactions $^{19}F(^3He,d)^{20}Ne$ [12] and $^{16}O(^7Li,t)^{20}Ne$ [13] these levels were found to be populated only weakly or not at all. We note that there is no direct experimental evidence of which we are aware that precludes the possibility of this being a 6p-2h band as predicted in the shell-model calculations of Ref. [14]. However, this band is now widely believed to have predominantly 8p-4h structure [15,16] similar to the shell model results of Ref. [17]. A more clearcut signature of 8p-4h structure would be the observation of significant strength in the α_1 decay

*Present address: P-17 MS H803, Los Alamos National Laboratory, Los Alamos, NM 87545.
†Present address: U.S.N.R.C., Region 1, 475 Allendale Rd., King of Prussia, PA 19406.

channel, since the first excited state of ^{16}O is believed [18,19] to have a predominantly 4p-4h character and can be thought of as an α cluster coupled to a ^{12}C core. More precisely, significant strength in the α_1 decay channel implies that the decaying level has a large overlap with an α cluster and ^{16}O in the first excited state. The α_1 decay channel is energetically closed for the excitation energies of the low-lying levels in the $K^\pi=0_3^+$ band. In the present work we focus on the experimental search for ^{20}Ne levels which have a strong decay to the α_1 channel. Such levels may be those which have two α-cluster degrees of freedom active. Theoretical models involving several cluster degrees of freedom have been proposed [15].

The starting point for this work was the discovery [20,21] of a $J^\pi=0^+$ level at $E_x=12.44$ MeV in ^{20}Ne with a large spectroscopic factor, $\Theta^2_{\alpha_1}\approx 1.15$ (we have corrected a factor of $\frac{3}{2}$ error in Ref. [21]) for decay to the first excited state of ^{16}O. Shell-model calculations were unable to account for such a large value. This discovery prompted a search for other ^{20}Ne levels which might belong in a rotational band headed by the 12.44 MeV level. Hindi *et al.* suggested [22,23] that a previously discovered [24] $J^\pi=6^+$ level at $E_x=15.16$ MeV and a $J^\pi=8^+$ level at $E_x=18.54$ MeV belonged to such a band. They based the assignments on the moderately large spectroscopic factors for decay of these states to the $J^\pi=2_1^+$ state in ^{16}O, which is a member of a band headed by the $J^\pi=0^+$ level at $E_x=6.05$ MeV in ^{16}O, and the large spectroscopic factor for ^8Be decay of the $J^\pi=8^+$ level. Richards *et al.* disputed [25] this conclusion and claimed that it would be more appropriate to assign these two levels to a band built on a $J^\pi=0^+$ level at $E_x=11.55$ MeV in ^{20}Ne that they [25] identified. Richards *et al.* also suggested that any ^{20}Ne levels belonging to the same rotational band as the $E_x=12.44$ MeV state should have similarly large α_1 spectroscopic factors. At the time the α_1 spectroscopic factor for the $J^\pi=6^+$ level was known to be less than a fairly small upper limit [26] and the α_1 branching ratio of the $J^\pi=8^+$ state had not been measured. One of the goals of this work is to determine values of the α_1 spectroscopic factor for both of these levels and to deduce whether or not they belong in a rotational band with the $J^\pi=0^+$ level at $E_x=12.44$ MeV.

Since we are interested in ^{20}Ne levels above the threshold for breakup into an α particle and ^{16}O in its first excited state, we have the opportunity to observe decays of ^{20}Ne levels into the α_1 channel directly. We have employed the reaction $^{16}O(\alpha,\alpha_1)^{16}O$, where the levels of interest are formed as resonances that decay to the first excited state of ^{16}O, as well as a sequential reaction, $^{12}C(^{12}C,\alpha)^{20}Ne^*$, in which ^{20}Ne levels are formed by the transfer of eight particles to a ^{12}C core and then decay into the α_1 channel. This two-pronged approach may be contrasted with earlier work in which states in ^{20}Ne below the threshold for $\alpha+^{16}O(0_2^+)$ breakup were suggested to have 8p-4h character on the basis of their strength in eight-nucleon transfer. The ability to observe the dominant component of the wave function by the direct decay of a resonant state should, we believe, permit a more quantitative elucidation of these core-excited levels than has been possible previously. The major effort in this work consisted of measuring the differential cross section of the $^{16}O(\alpha,\alpha_1)^{16}O$ reaction over the range of bombarding energies $10.2\le E_\alpha\le 18$ MeV in which we identified events populating the first excited state of ^{16}O by requiring a coincidence with an electron or positron from the $E0$ decay of that state by internal pair emission. In contrast to past experiments [27] we measured cross sections, in most cases, at a sufficient number of angles to allow a complete parametrization of the angular distributions in terms of Legendre polynomials. We used the $^{12}C(^{12}C,\alpha)^{20}Ne^*$ reaction to measure the α_1 branching ratios of the $J^\pi=6^+$ and 8^+ levels suggested as candidates for a band with the $J^\pi=0^+$ level at $E_x=12.44$ MeV since this reaction is known to excite them. We identified α_1 decays of ^{20}Ne by requiring the coincident observation of an electron or positron.

In addition to its unusual structure, the $^{16}O(0_2^+)$ decay channel presents an opportunity that is not usually found in studies involving decays of resonances to low-lying excited states. Because the first excited state of ^{16}O as well as the α particle both have an intrinsic angular momentum of $0\hbar$, only resonances with parity $=(-)^J$ can be formed; also, resonances of spin J in ^{20}Ne can decay to the 0_2^+ channel only by a single partial wave with $l=J$. This fact simplifies the analysis compared to the case where several l values can contribute to the decay of a single level.

II. EXPERIMENTAL PROCEDURE

A. $e^\pm$ detector

A common feature of the experiments reported here is that the final state in each case included ^{16}O in the first excited state ($E_x=6.05$ MeV, $J^\pi=0^+$). In both experiments, we identified this state by observing electrons or positrons from its internal pair decay. In the case of the $^{16}O(\alpha,\alpha_1)^{16}O$ experiment this was necessary because the second excited state in ^{16}O, $J^\pi=3^-$, lies only 80 keV higher in excitation energy and α decays to the two levels are not resolvable in solid-state detectors because of the low energy available in the exit channel. We exploited the fact that the first excited state in ^{16}O decays [28,29] nearly 100% of the time by the emission of an electron-positron pair. This is in contrast to the $J^\pi=3^-$ state which decays almost 100% of the time by γ emission [30].

The electron detector used in this experiment consists of a thin (0.4 mm) anthracene crystal and a photomultiplier tube similiar to the device described in Ref. [31]. Photons produced in the anthracene are transported to a photomultiplier tube by an air light guide. The efficiency for the detection of electrons or positrons from the decay of the $J^\pi=0^+$ level in ^{16}O is maximized by making the solid angle subtended by the detector large. The diameter of the anthracene crystal is 6.5 cm; its center is placed approximately 2.5 cm from the target.

In Ref. [31] a figure of merit, R, for the detector performance was defined by

$$R = \frac{\epsilon_\pi}{\epsilon_\gamma} ,$$

where ϵ_π is the efficiency for detecting an electron or positron or both from the monopole decay of the first excited state in ^{16}O and ϵ_γ is the efficiency for detecting gamma rays from the decay of the first $J^\pi=3^-$ level in ^{16}O. ϵ_γ is dependent on the particle-gamma angular correlation and the geometry of the scattering chamber [3] whereas ϵ_π is not. The electron detector can be thought of as a device that supresses the reactions leading to the $J^\pi=3^-$ state by a factor of R relative to reactions leading to the first excited $J^\pi=0^+$ state. In the $^{12}C+^{12}C$ branching ratio measurements, where we measure small α_1 branching ratios, a large value of R is important. Efficiency measurements of ϵ_π were made using the technique outlined in Ref. [31] as a part of each of the experiments presented in this work. In the case of the $^{12}C+^{12}C$ experiment we ran the efficiency measurements for an extended period so that we could also measure ϵ_γ accurately and therefore deduce a value for R. In this case we found ϵ_π to be 0.3775 ± 0.0045 and the value of R to be 109 ± 28. The relatively lower precision obtained in measuring R results from the intrinsically low efficiency of the thin scintillator for γ rays and the correspondingly poorer statistical accuracy.

B. The $^{16}O(\alpha,\alpha_1)^{16}O$ measurements

The goal of the $^{16}O(\alpha,\alpha_1)^{16}O$ experiment is to obtain inelastic scattering data from $E_\alpha \approx 10$ MeV, which is the high end of the energy range of Ref. [21] to $E_\alpha \approx 18$ MeV, above which the α_1 cross sections have been previously measured by Billen [32] and Riedhausser [33]. We have taken data in 25 keV steps over most of this energy range. During most of the $^{16}O(\alpha,\alpha_1)^{16}O$ experiment, we used detectors at fifteen angles spanning the range of laboratory angles 17.5° to 162.5°. Laboratory solid angles subtended by the detectors ranged from 0.36 msr at the most forward angles to 1.35 msr at back angles. There were two regions, 11.75–12.75 and 14.75–15.75 MeV, which we, *a priori*, deemed to be particularly important where we have taken data with two different placements of the fifteen detectors for a total of 26 different angles (some detector positions in the second setting corresponded to the position of a different detector in the first setting). The targets were self-supporting SiO_2 foils with a nominal thickness of 40 $\mu g/cm^2$ which corresponds to beam energy losses in the target on the order of the step size.

At each energy and angle particle energy spectra were recorded both in singles and in true coincidence with the electron detector. The coincidence spectrum was generated by producing a spectrum gated on the true peak in a time difference spectrum and subtracting from it a spectrum of accidental coincidences. Figure 1 illustrates a time difference, singles, and true coincidence spectrum for $E_\alpha=15$ MeV and $\theta_{lab}=57.5°$. Because we did not record the data in event-by-event form, we did not include a contribution from the background in the uncertainties for each data point. As can be seen from the time

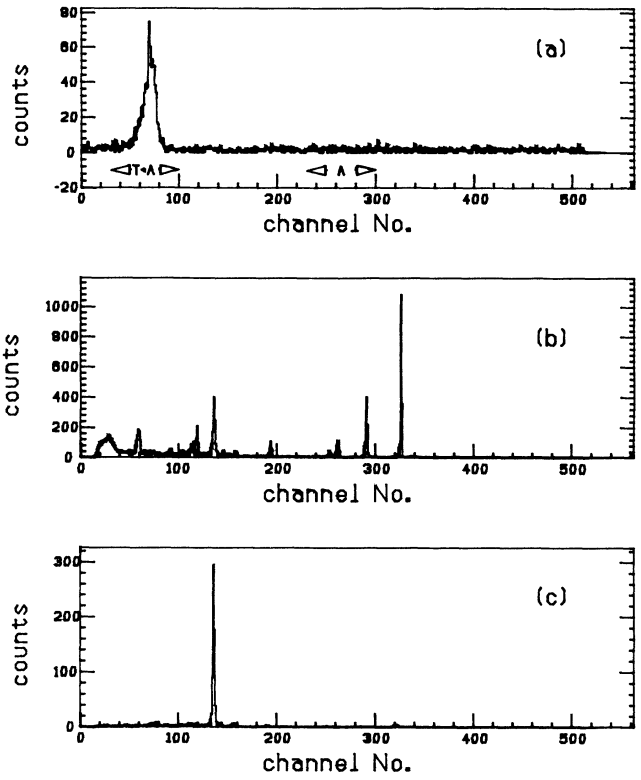

FIG. 1. Example of data from $^{16}O(\alpha,\alpha_1)^{16}O$ experiment at $E_\alpha=15$ MeV and $\theta_{lab}=57.5°$. (a) TDC histogram, (b) singles histogram, (c) coincidence histogram.

difference spectrum, which is typical, the accidental coincidence rate in this experiment was quite low. Since the accidental contribution to the true peak represents counts spread throughout the pulse-height spectrum, the contribution to the errors from background is negligible.

The target thickness was established by summing the peaks corresponding to elastic scattering from ^{16}O in the singles spectra in a narrow energy region around 13 MeV. By comparing the sums with published elastic cross sections [34] we established a relative normalization. The comparison of the elastic scattering data was done at 13 MeV because the cross section as a function of energy is relatively unstructured there; small differences in the energy calibrations between the University of Wisconsin and University of Pennsylvania accelerators or energy losses in targets should therefore not affect the comparisons. We followed this procedure because the Wisconsin data [34] was taken with a high purity gas cell in which the ^{16}O thickness was believed to be well known. This enabled us to avoid uncertainties arising from foil target stoichiometry.

Linear and logic signals for each surface barrier detector were processed by a combination of commercial NIM and CAMAC electronics and an eight-channel charge sensitive preamplifier module coupled to an eight-channel amplifier/discriminator module. Both eight-channel modules were constructed for this experiment [35]. The data were histogrammed directly into the memory of the

University of Pennsylvania parallel-processing computer system [36].

We assign an uncertainty to the overall normalization of the $^{16}O(\alpha,\alpha_1)^{16}O$ cross sections of 7%, which results from adding the uncertainty of the relative normalization of our elastic data to the Wisconsin data (6%), the uncertainty in the overall normalization of the Wisconsin data (2%), and the uncertainty in the electron detector efficiency (3%) in quadrature. In addition there could be a slow variation with beam energy in the electron detector efficiency of about 4% because of the motion of the beam spot on the target resulting from point to point differences in the beam tune. We estimate the uncertainty in the beam energy to be about 0.1%, the uncertainty in the detector laboratory angles to be about 0.5°. The relative solid angles subtended by the detectors were checked by positioning an ^{241}Am source (which emits α particles isotropically) in the target position. Relative solid angle uncertainties are estimated to be 4%, mostly due to uncertainties in postioning the source.

The cross sections for the $^{16}O(\alpha,\alpha_1)^{16}O$ reaction are tabulated in the appendix of Ref. [35]. Figure 2 is a plot of the average cross section at each energy extracted from the angular distributions by linear fits by Legendre polynomials, some of which are illustrated in Fig. 3. We find the energy dependence of the measured cross sections to be in good agreement with the results of Garman [27] at the angles where a comparison can be made; the overall normalization in Ref. [27] is lower than ours by a factor between 0.5 and 0.6. Caskey [34] was able to separate the $^{16}O(\alpha,\alpha_1)^{16}O$ from $^{16}O(\alpha,\alpha_2)^{16}O$ channels for a single angle over the energy range 12.45–13.47 MeV. Except for the very highest part of this region, both the energy dependence and overall normalization of the data of Ref. [34] and the present work agree within errors. The slight discrepancy at the high end of the region may be due to the fact that the $^{16}O(\alpha,\alpha_2)^{16}O$ cross section is large there, making the extraction of the $^{16}O(\alpha,\alpha_1)^{16}O$ peak in a singles experiment such as that of Ref. [34] difficult.

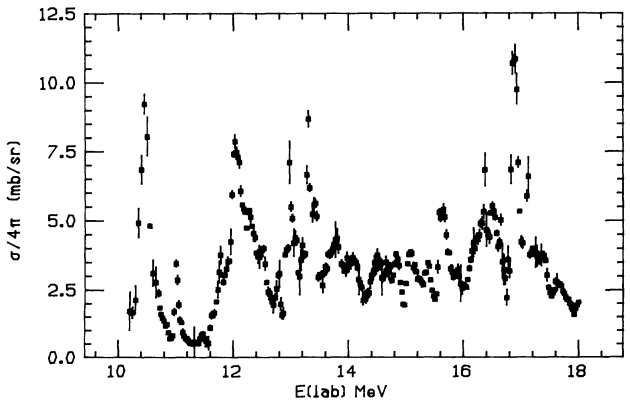

FIG. 2. Average cross section as a function of energy for the reaction $^{16}O(\alpha,\alpha_1)^{16}O$ derived from the fits to the data as explained in the text.

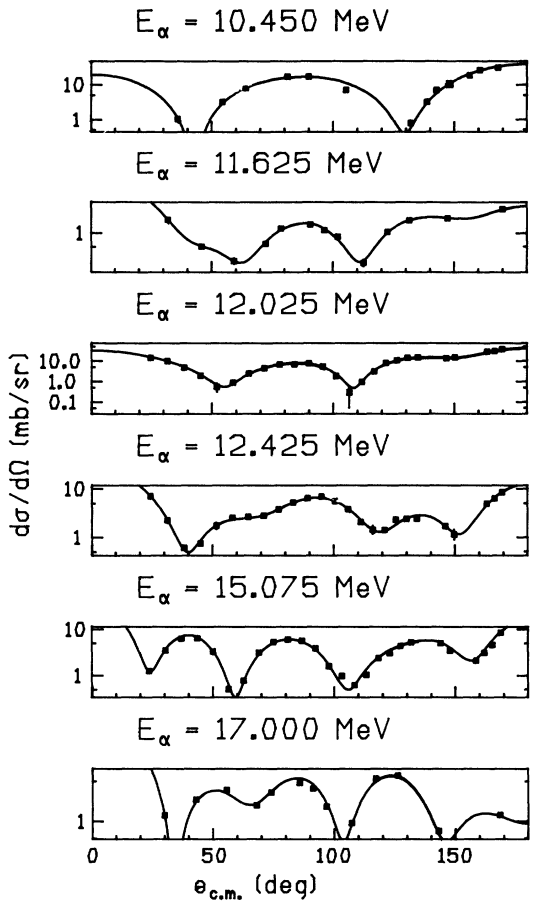

FIG. 3. Some angular distributions for the reaction $^{16}O(\alpha,\alpha_1)^{16}O$. Lines represent a Legendre polynomial fit to the data as described in the text.

C. The $^{12}C(^{12}C,\alpha)^{20}Ne^* \rightarrow \alpha_1 + {}^{16}O^*$ measurements

The goal of the $^{12}C+^{12}C$ experiments is to populate levels in ^{20}Ne by the direct transfer of 8 nucleons to a ^{12}C core. The reaction was chosen because, in the direct reaction model, it is likely to populate selectively 8p-4h levels. In this experiment, a ^{12}C beam interacted in a thin (nominally 25 $\mu g/cm^2$) isotopically enriched ^{12}C target. Alpha particles emitted at 0° signaling the formation of excited levels in ^{20}Ne were focused by a quadrupole singlet with an effective solid angle of approximately 8 msr and dispersed in momentum by a 65 cm Spectromagnetic Industries magnetic spectrometer [37] and detected by a position sensitive silicon surface barrier detector [24]. Coincidences between α particles in the forward direction and the electron detector described above were used to identify those events which involve the first excited state of ^{16}O. Bombarding energies of 36.3 and 61 MeV were used in the $^{12}C+^{12}C$ experiment.

III. RESULTS AND ANALYSIS

Since a primary goal of this work is to identify candidates for a rotational band based on the $J^\pi=0^+$ level at

$E_x = 12.44$ MeV, we have arranged the discussion of individual resonances according to the spin of the ^{20}Ne compound system. Most of the results come from the $^{16}O(\alpha,\alpha_1)^{16}O$ experiment. The $^{12}C+^{12}C$ branching ratio measurements are used in discussion of the $J^\pi = 6^+$ and 8^+ levels.

A. Formalism

A multilevel resonance formalism, such as R-matrix theory [38], can be used to extract resonance parameters from the inelastic scattering cross sections. The task of fitting the data is greatly simplified (especially in the case of zero channel spin in both incoming and outgoing channels) if one can first separate the contributions of the different partial waves that contribute to the cross section.

A technique [35,39–41] for finding the multiple sets of partial wave amplitudes that yield the observed cross section proved useful and is briefly outlined here. Since the reaction $^{16}O(\alpha,\alpha_1)^{16}O$ has channel spin zero in both the incoming and outgoing channels, the differential cross section can be written as the square of a scattering amplitude formed from a sum of Legendre polynomials:

$$\frac{d\sigma}{d\Omega}(E,\theta) = f(\theta)f^*(\theta) = \left| \sum_{l=0}^{l_{\max}} B_l(E) P_l(\cos\theta_{\text{c.m.}}) \right|^2 , \quad (1)$$

where the B_l are complex partial wave amplitudes and $l_{\max}$ is the order of the maximum contributing partial wave amplitude. We find the B_l, or, equivalently, the functional form of $f(\theta)$ at each energy, by expressing the cross section in terms of its complex roots:

$$\frac{d\sigma}{d\Omega} = N \prod_{i=1}^{l_{\max}} (x - x_i)(x - x_i)^* = N \prod_{i=1}^{l_{\max}} (x - x_i)(x - x_i^*),$$

where $x = \cos\theta$ and the x_i are the roots. The factors appear in complex conjugate pairs because $d\sigma/d\Omega$ is a real, nonnegative function.

A possible scattering amplitude is

$$f(\theta) = \sqrt{N} e^{i\phi} \prod_{i=1}^{l_{\max}} (x - x_i) ,$$

where ϕ is an arbitrary phase independent of scattering angle. Other scattering amplitudes can be formed by taking x_i^* instead of x_i in any of the factors in the above equation. In the expression for f, there are $l_{\max}$ factors, each of which can have two possible values, $(x - x_i)$ or $(x - x_i^*)$, so that in addition to an overall phase ambiguity there are $2^{l_{\max}}$ possible forms of the scattering amplitude (sets of B_l), of which half are complex conjugates of the other half. Except for an overall phase, $B_{l_{\max}}$ is unique. To make use of this technique, one must parametrize the data in some form. We have chosen to fit our data by Eq. (1) so that, at each energy a particular set of the B_l is found from which we generate the others. One can also fit the data by a linear sum of Legendre polynomials,

$$\frac{d\sigma}{d\Omega}(E,\theta) = \sum_{l=0}^{2l_{\max}} A_l(E) P_l(\cos\theta_{\text{c.m.}}). \quad (2)$$

Although we use this equation to find $l_{\max}$, we have not used it in the actual parametrization of the data because the range spanned by Eq. (2) includes unphysical regions. For example, without perfect data such a fit could, in principle, yield a set of values of A_l which yield negative cross sections at some angles. We have chosen instead to fit by Eq. (1) because its range corresponds exactly to the physically allowed region.

The problem now is to find a method to connect the various amplitudes from energy to energy and then of selecting the correct solution. Usually the solutions are connected based on some sort of smoothness criterion and the correct solution is picked by comparing the behavior of the different possibilities with that expected based on a reaction model. This process can be very difficult, even with $l_{\max}$ as small as 3. In the present case we focus on extracting the cross section due to the highest contributing partial wave, for which a unique determination is always possible, or the second highest partial wave. In the latter situation, we restrict our attention to cases where its contribution to the total cross section dominates that from the highest partial wave. Under these circumstances, all of the possible solutions at each energy group together, so that linking them from energy to energy is not necessary and usually not possible. Instead we resolve the ambiguity by averaging all the possibilities together at each energy as described in Sec. III B.

We performed multilevel three channel R-matrix [38] fits to the cross sections for individual partial waves extracted by the above procedure. We find the expression for a general off diagonal element W_{12}, where the collision matrix $U = \Omega W \Omega$, and Ω is a diagonal matrix containing the hardsphere and Coulomb phases, in the case of three channels to be

$$W_{12} = \frac{2i(P_1P_2)^{1/2}}{D}(R_{12} + R_{13}R_{23}L_3^0 - R_{12}R_{33}L_3^0) ,$$

where

$$D = 1 - (c_{12}^2 + c_{13}^2 + c_{23}^2) + c_{11}c_{22} + c_{11}c_{33} + c_{22}c_{33} - c_{11}c_{22}c_{33} - 2c_{12}c_{13}c_{23} + c_{11}c_{23}^2 + c_{22}c_{13}^2 + c_{33}c_{12}^2$$

and $c_{ij} = R_{ij}(L_i^0 L_j^0)^{1/2}$. The definitions of the R-matrix parameters are given in Ref. [38]. In this expression channel one is the elastic entrance channel and channel two is the exit channel. In the present case there are open channels in addition to the elastic and inelastic excitation of the 0_2^+ level. The present data are not able to determine the partitioning of the available flux into these channels, so we have added a third channel to account

for the diversion of flux into all other open channels.

The actual parameters in R-matrix theory are the resonance energies E_λ and the reduced width amplitudes $\gamma_{\lambda c}$. Often in the disscusion of the data analysis we will refer to channel widths and total widths, which are not R-matrix parameters. In presentation of fit results, these quantities should be understood to mean

$$\Gamma_{\lambda c}=2\gamma_{\lambda c}^2 P_c|_{E=E_\lambda}, \qquad \Gamma_\lambda=\sum_c \Gamma_{\lambda c}.$$

We defined the $\Gamma_{\lambda c}$ to be constants to agree with often made approximations in R-matrix theory; however, in the actual fits, the parameters used were the $\gamma_{\lambda c}$ directly. The energy dependence of the elastic and inelastic penetrabilities were therefore included automatically.

The parameters involved in an R-matrix fit include reduced width amplitudes for all channels considered. In the present case the elastic amplitudes were taken from previously published analyses of elastic scattering data rather then undertaking an *ab initio* analysis of the elastic scattering data acquired in the present experiment. As mentioned, from the inelastic scattering data we extracted the contributions of individual partial waves to the cross section. Since elastic scattering involves partial waves of all orders, we cannot apply the same technique to the elastic data. Although it may be possible to perform a partial wave decomposition of the elastic scattering by explicitly including calculated Coulomb scattering, this would require data at more angles in some energy regions then we have in our data set. This is because for a given bombarding energy, the kinetic energy in the α_0 channel is 6.05 MeV higher than in the α_1 channel and therefore one sees contributions to the nuclear part of the cross section from higher-order partial waves in the elastic channel than in the inelastic. The present analysis should thus be viewed as more of a search for concentrations of α_1 decay strength then as the most rigorious R-matrix analysis possible.

B. $J^\pi=2^+$ level

Our data show a large structure at a bombarding energy of about 10.45 MeV and the angular distributions shown in Fig. 3 for energies in this region show a strong $|P_2(\cos\theta)|^2$ dependence. By fitting the angular distributions to linear sums of Legendre polynomials, we found that partial waves above $l=3$ do not make significant contributions to the cross section. The partial wave amplitudes were extracted from the data and are presented in Fig. 4 where, for each l value we plot $B_l^2/(2l+1)$ versus energy. This quantity is proportional to the contribution to the total cross section due to a particular l value, i.e., the cross section that would result if we could turn off all other partial waves. The fact that the $l=2$ cross section possibilites group together is a result of the contribution from the $l=3$ (l_{max}) partial wave being much smaller than that from the $l=2$ ($l_{max}-1$) partial wave. This grouping allows us to generate an effective cross section by averaging the possibilities at each energy. Note that this method would not be useful for $l<2$. The effective $l=2$ cross sections resulting from this procedure

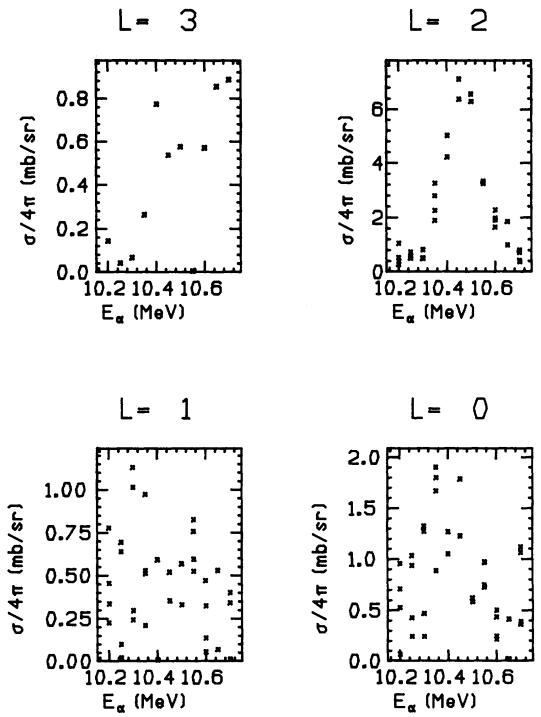

FIG. 4. Plots of all possible effective average cross sections for all values of l derived from the $^{16}O(\alpha,\alpha_1)^{16}O$ data from 10.2 to 10.7 MeV.

are shown in Fig. 5. The yields have been converted to differential cross sections for ease of use with our R-matrix fitting routine. The error bars represent the standard deviation in the spread of the points combined in quadrature with the errors from the fits to the angular distributions used to generate the partial wave decomposition.

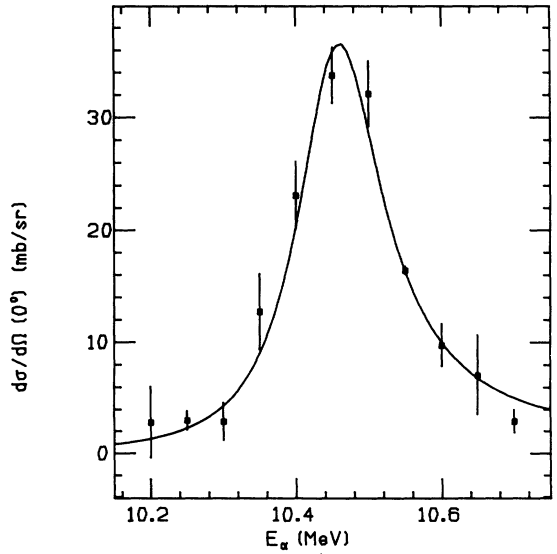

FIG. 5. Results of an R-matrix fit to the average of the effective $l=2$ cross sections.

A recent compilation [30] lists one $J^\pi=2^+$ level seen in elastic scattering in this region at $E_\alpha=10.283\pm0.002$ MeV. This state is about 180 keV away from the peak of the inelastic cross section so it is unlikely that the two levels are the same. We did not include the level in the R-matrix fit because it is reported to have a 100% α_0 branch and we were able to fit the data without it.

For a single level with 0 channel spin, the differential cross-section formula reduces to

$$k^2\frac{d\sigma}{d\Omega}=\frac{(2l+1)^2}{4}\frac{\Gamma_{\alpha_0}\Gamma_{\alpha_1}}{[E_\lambda-(E-\Delta)]^2+\Gamma^2/4}P_l(\Omega)\ , \qquad (3)$$

where Γ_{α_0} and Γ_{α_1} and therefore Γ are energy dependent through the penetrabilities and Δ is also energy dependent:

$$\Gamma_i=2P_i\gamma_i^2,$$

$$-\Delta_i=[S_i(E)-B_i]\gamma_i^2=S'_i(E)\gamma_i^2,$$

and

$$\Delta=\sum_i\Delta_i\ .$$

Here, $\Gamma=\sum_i\Gamma_i$ and γ_i is an R-matrix reduced width amplitude. P_i, the penetrability in channel i, is minus the imaginary part of the logarithmic derivative of the outgoing wave function and therefore consists of Coulomb quantities. Similiarly S_i, the shift function, is the real part. B_i is the (real) boundary condition value and can be chosen once in each channel. We have chosen $B_i=S_i(E_\lambda)$ so that $S'_i(E_\lambda)=0$. There exists a continuum of R-matrix parameters that will produce fits to the data of similiar quality. Mathematically, the minimum possible value for $\Gamma_{\alpha_1}|_{E=E_\lambda}$ consistent with the observed cross section in the α_1 channel occurs when the total width of the state is exhausted by the α_0 and α_1 channels, i.e., when $\Gamma_{\alpha_0}(E)+\Gamma_{\alpha_1}(E)=\Gamma(E)$. With the fitting routine constrained to meet this condition we find the resulting laboratory values of the parameters to be $\Gamma_{\alpha_1}|_{E=E_\lambda}=50.5\pm4.1$ keV, $\Gamma_{\alpha_0}|_{E=E_\lambda}=151\pm15$ keV, and $E_\lambda=10.456\pm0.005$ MeV. The center-of-mass value of Γ_{α_1} is 40.4 ± 3.3 keV. The errors quoted represent 1σ as measured by the change in χ^2 of the fit. The fit is illustrated by the line in Fig. 5. This result for Γ_{α_1} is spectroscopically useful because even the minimum value found corresponds to a large overlap of the resonance with the α_1 channel.

At low energies, the observed full width at half maximum W of a level is dramatically affected by the change in the shift function S with energy. If we assume that most of the effect comes from the inelastic channel, we find

$$W\approx\frac{\Gamma|_{E=E_\lambda}}{1+A\Gamma_{\alpha_1}|_{E=E_\lambda}/2P_{\alpha_1}}\ ,$$

where

$$A=\frac{\partial S'_{\alpha_1}}{\partial E}\bigg|_{E=E_\lambda}\ .$$

The value of W in the center-of-mass system for the present fit, 115 ± 10 keV, is in fact much less than Γ which illustrates this point.

Caskey [34] reports a structure in the elastic data at about 10.46 MeV that, by visual inspection, is consistent with several possible spins, including $J^\pi=2^+$. He assigned the spin and parity as $J^\pi=6^+$, found a center-of-mass width of 102 ± 5 keV, and an elastic branching ratio of 52%. This width is close to the value of W that we observed for the $J^\pi=2^+$ level under consideration, so it is possible that the level observed in elastic scattering and assigned a spin of $J^\pi=6^+$ is actually the $J^\pi=2^+$ level that we observe in the α_1 channel.

The spectroscopic factor or dimensionless reduced width is defined as

$$\Theta_i^2=\frac{\Gamma_i}{\Gamma_{\text{s.p.}}}\ ,$$

where

$$\Gamma_{\text{s.p.}}=2P_i\gamma_{WL}^2.$$

P_i is a penetrability and

$$\gamma_{WL}^2=\frac{3}{2}\frac{\hbar^2}{\mu_c a_c^2}$$

and is known as the Wigner limit. It is an upper limit on the R-matrix reduced width and depends only on the channel partition through the reduced mass and channel radius. We assume a channel radius of 5.75 fm which results in a value of γ_{WL}^2 of 592 keV in the center-of-mass system. We conclude that $\Theta_{\alpha_1}^2>0.63$, corresponding to the limiting value of 37.1 keV for Γ_{α_1} as obtained from the value 40.4 ± 3.3 keV resulting from the fit.

The striking feature of this state is its large value of $\Theta_{\alpha_1}^2$ which indicates that there is a large overlap between this $J^\pi=2^+$ state in ^{20}Ne and the final state, $^{16}\text{O}(J^\pi=0_2^+)+\alpha$. A large value of $\Theta_{\alpha_1}^2$ is also a property of the $J^\pi=0^+$ level in ^{20}Ne at $E_x=12.44$ MeV.

C. $J^\pi=4^+$ levels

In this section we discuss the results of the $^{16}\text{O}(\alpha,\alpha_1)^{16}\text{O}$ experiment in the range of bombarding energies $11.20<E_\alpha<12.75$ MeV. In this region we have 25 point angular distributions from 11.75 to 12.75 MeV and 13 to 15 point angular distributions everywhere else. Data were taken in 25 keV steps. Garman's [27] work shows complicated structure over the 1 MeV range where we have taken our 25 point angular distributions. This is also the region where one might expect to find the $J^\pi=4^+$ member of a rotational band that contains the $J^\pi=0^+$ state at $E_x=12.44$ MeV and the $J^\pi=2^+$ level just discussed.

The structure of the angular distributions (Fig. 3) in this energy region is more complicated than in the

preceding case; several partial waves are making significant contributions to the cross section. Fits to linear sums of Legendre polynomials show that partial waves above $l=5$ do not make significant contributions to the cross section.

In Fig. 6 we plot the multiplicity of possible $l=4$ cross sections as a function of energy and we see that the possibilities are fairly tightly bounded. We treat this partial wave by averaging the cross sections corresponding to different solutions at each energy, just as we did in the case of the $J^\pi=2^+$ level. The data points shown in Fig. 7 are the effective average $l=4$ cross sections obtained in this way.

In this region several $J^\pi=4^+$ levels are known from elastic scattering [30]. In order to use these parameters we must establish an energy calibration between our accelerator and the University of Wisconsin machine. At the energies discussed in this section, the most convenient way to do this is to note that Caskey [34] has separated the $^{16}O(\alpha,\alpha_1)^{16}O$ from $^{16}O(\alpha,\alpha_2)^{16}O$ cross sections for $\theta_{lab}=40°$ over the range $12.4<E_\alpha<13.45$ MeV. Comparing our data with his, we find that the Wisconsin calibration is 13±8 keV lower than ours at $E_\alpha=12.5$ MeV. We have made a correction for target thickness in obtaining this number.

In the fits to be described we allow the parameters known from elastic scattering (the elastic branching ratios, total widths, and resonance energies corrected by 13 keV) to vary by twice the uncertainty quoted in Ref. [30]. We try all possibilities for the sign of the elastic reduced widths for known levels and start the elastic reduced widths of new levels (levels not previously reported) as well as all the inelastic reduced widths at zero.

The dashed line in Fig. 7 shows the best result obtained by using the states known from elastic scattering [30] including the two uncertain levels. By experimenting with

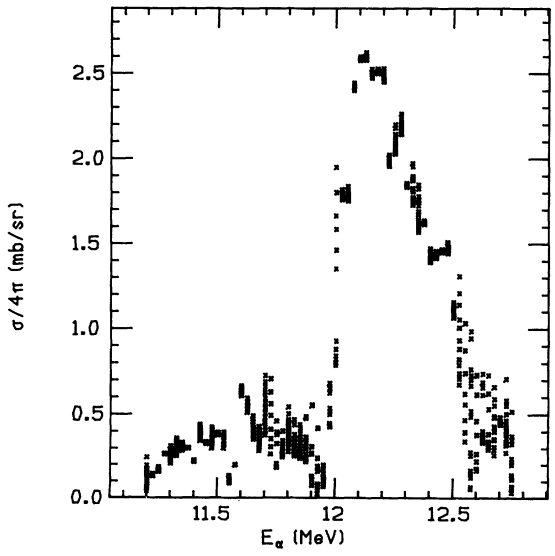

FIG. 6. Plots of all possible effective average cross sections for $l=4$ derived from the $^{16}O(\alpha,\alpha_1)^{16}O$ data from 11.2 to 12.75 MeV.

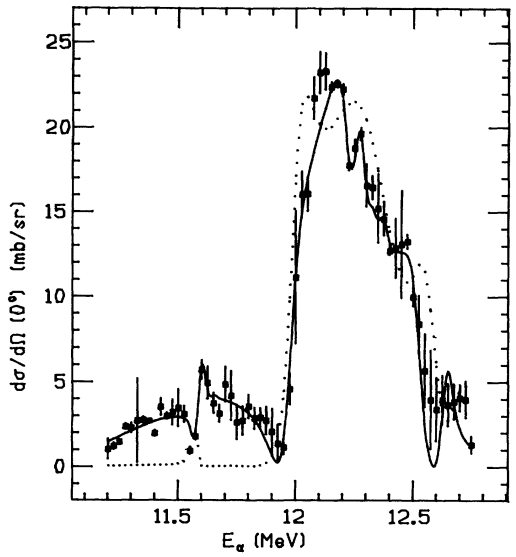

FIG. 7. Fits by the averaged $l=4$ effective cross sections using the five levels deduced from the $^{16}O(\alpha,\alpha_0)^{16}O$ reaction (dashed) and using three additional levels (solid).

the addition of various new levels, we find that we can reproduce most of the structure in the data by adding three new states. The solid line in Fig. 7 shows the best results from these fits.

An important difference between the analysis of this section of the data and the previous 2^+ region is that in the 2^+ region we could deduce all the sets of R-matrix parameters that yield fits to the data from a single fit. This is no longer possible since we now have several overlapping levels. Our interest lies in determining the overlap of the states in this region with the $^{16}O(0_2^+)+\alpha$ channel. We therefore concentrate our efforts on determining a value (or at least limits) for the sum of the inelastic spectroscopic factors $\sum_i \Theta^2_{\alpha_1,i}$, where i labels the $J^\pi=4^+$ levels in this region; this is the quantity which contains the nuclear structure information.

Figure 7 is the result of an R-matrix fit to the data. We ran many such fits to map out the parameter space. Reference [35] contains a list of all the parameter sets we found that produce a fit to the data of a quality close to that shown in Fig. 7. The individual parameter sets obtained from the fits are not meaningful but must be viewed as a whole. We have excluded from consideration any fits in which levels not previously seen in the elastic scattering analysis [34] yielded an elastic branching ratio of greater than 40% since levels with a large elastic branch should have presumably been identified in the elastic scattering study. The cutoff value is large because there is a broad $J^\pi=4^+$ level seen in elastic scattering that could mask the effects of other (4^+) levels lying nearby. An exception to the 40% rule occurs when the total width of a new state is greater than 400 keV (laboratory) since such a broad level may have been treated as background in the elastic analysis.

Several results have emerged from this analysis. In all

twelve acceptable fits to the data, the sum of the inelastic spectroscopic factors is large. In all the cases except one the summed spectroscopic factor is greater than 1. The only fit that has a value of $\sum_i \Theta^2_{\alpha_1,i}$ less than 1 is a case where we have allowed a wide level to have an elastic branching ratio greater than 40%. We conclude that the value of $\sum_i \Theta^2_{\alpha_1,i}$ for 4^+ states in the laboratory energy range 11.2–12.75 MeV is greater than 0.5 and probably is close to 1. Finally, we cannot fit the data without the addition of at least three levels (whose specific properties vary from fit to fit) not reported in the elastic scattering analysis.

D. $J^\pi = 6^+$ and 8^+ levels

An examination of the data shows possible $l=6$ structure in the region $E_\alpha = 15$ to 17.5 MeV. In this region we have data spaced in 25 keV steps. Between 14.75 and 15.75 MeV the angular distributions consist of 26 points, elsewhere they contain 13 to 15 points. This is the second of the two regions where high density angular distributions were taken. Extra experimental attention was paid to this region because earlier data [27] show complicated structure in this energy range and it is where one might expect to find a $J^\pi=6^+$ level with similar structure to the $J^\pi=0^+$ state at $E_x=12.44$ MeV and the previously discussed $J^\pi=2^+$ level at $E_x=13.1$ MeV.

Linear fits to Legendre polynomials show this region to have a maximum l value of 6 up to $E_\alpha=15.75$ MeV. Above this energy there are too few data points in the angular distributions to determine $l_{\max}$. We assume that $l_{\max}=6$ over the entire region. Since the amplitude resulting from the maximum contributing partial wave is unique, we can extract (within a phase) the $l=6$ partial wave at $E_\alpha=15.75$ MeV and below by fitting to Eq. (1). Above 15.75 MeV, the fits are underconstrained because of the shortage of data points We addressed this problem by taking the resultant parameters of the fit at 15.75 MeV, where we know that we do not have a problem with inequivalent fits, and using them as the starting values of the fit for the first point above 15.75 MeV and then taking the result of this fit as the starting parameters for the next point, etc. This procedure is likely to give "correct" results near 15.75 MeV; it is possible that we are generating "incorrect" fits once we get some distance away. The lines in Fig. 8 are the results of the fits. We checked our results at high energies by running fits with different starting parameters and comparing the results. We find that the $l=6$ cross section generated from the various fits always shows the same main structures although some of the details vary from fit to fit.

An energy calibration between our data and the Wisconsin data was established by comparing elastic scattering cross sections from 14.6 to 14.8 MeV for center-of-mass angles around 114°. We found the Wisconsin energy calibration to be 20±10 keV lower than ours.

The ^{20}Ne levels with $J^\pi=6^+$ known from elastic scattering are listed in Ref. [30]. The parameters of all the levels listed had their origin in the Wisconsin analysis

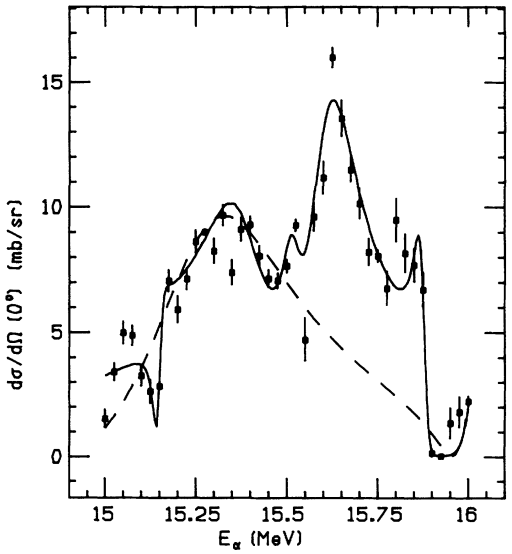

FIG. 8. Fit by the effective $l=6$ cross section of region A using the three levels deduced from the $^{16}O(\alpha,\alpha_0)^{16}O$ reaction (dashed) and using five additional levels (solid).

[42] so we corrected their energies by 20 keV in the fits to be described. Because of the large number of resonances, we divided this region into two sections for analysis. The first (A) is shown in Fig. 8 and includes the energies from 15 to 16 MeV and the second (B) is shown in Fig. 9 and runs from 16 to 17.5 MeV. Section A is derived mainly from our high-quality data while B comes from our poorer data.

Our first attempt at fitting the extracted $l=6$ cross section from the data in region A is shown as the dashed line

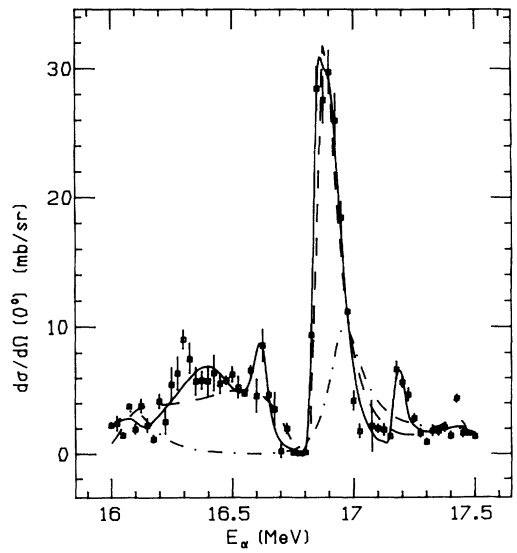

FIG. 9. Fit by the effective $l=6$ cross section of region B using three levels deduced from the $^{16}O(\alpha,\alpha_0)^{16}O$ reaction (dot-dashed), using four $^{16}O(\alpha,\alpha_0)^{16}O$ levels (dashed), and using four $^{16}O(\alpha,\alpha_0)^{16}O$ levels and four additional (solid).

in Fig. 8 where we included only the three levels known from elastic scattering and no others. The solid line in Fig. 8 is the result of fitting the data with the three levels known from elastic scattering and five additional levels. In mapping out the parameter space, we found a total of 4 sets of parameters that yield fits of a quality similiar to that shown in Fig. 8. In order to be accepted the new levels had to have elastic branching ratios of less than 30% unless the total laboratory width was greater than 500 keV. All of the accepted fits yield a value of $\sum_i \Theta^2_{\alpha_1,i}$ greater than 12%.

We follow the same procedure in region B with one exception. The resonance energies of states known from the elastic analysis are allowed to vary by twice the uncertainty quoted in Ref. [30] or by the uncertainty in Ref. [30] with an additional 20 keV, whichever is greater. This extra freedom is allowed because we are now some distance away from 14.8 MeV, where we checked the relative calibration of the University of Wisconsin and University of Pennslyvania data. (There are no good places in this region to make such a comparison.) In practice this extra freedom only applied to one state.

In our first attempt to fit the data with only those states known from elastic scattering we did not include the state at 18.03 MeV. The result is shown as the dot-dashed line in Fig. 9. The dashed line is the best result when we did include the level. Although this fourth elastic level is significantly outside the fitting range, the interference effects between it and the other levels are clearly important. In all that follows we have included state as one of the known elastic levels.

The solid line in Fig. 9 illustrates the best fit that we obtained by using four new levels in addition to the four elastic levels. All parameters that produced acceptable fits are listed in Ref. [35]. We find that the lowest value of $\sum_i \Theta^2_{\alpha_1,i}$ obtained from eight level fits to region B is 18%.

Over the combined energy range 15 to 17.5 MeV there is considerable structure. We have shown that although we cannot find a set of resonance parameters which uniquely fits all of the data, we can establish a lower limit on $\sum_i \Theta^2_{\alpha_1,i}$ of 0.12 + 0.18 =0.30. We also see that this strength may be divided up over many states spanning a large energy region, in contrast to the $J^\pi=2^+$ level at $E_\alpha=10.47$ MeV or the 0^+ state at $E_\alpha=9.64$ MeV [21].

It is also important to consider the possibility of additional 6^+ strength at lower bombarding energies. Figure 10 shows a strong, narrow peak in our data at about $E_\alpha=13.3$ MeV that is also apparent in the work of Garman [27] who tentatively assigned it a spin of 0 or 6. The level is clearly evident in the effective $l=6$ cross section, which can be obtained directly from the data since $l=6$ is the highest contributing partial wave. Therefore we can make a definite $J^\pi=6^+$ spin assignment. No $J^\pi=6^+$ levels are known at this energy in ^{20}Ne so we have fit the peak as a single level, as in the case of the $J^\pi=2^+$ level, without the benefit of elastic scattering results. The observed width of this level (about 30 keV in the laboratory) is small enough compared to the step size that additional parametrization of the background would not be useful.

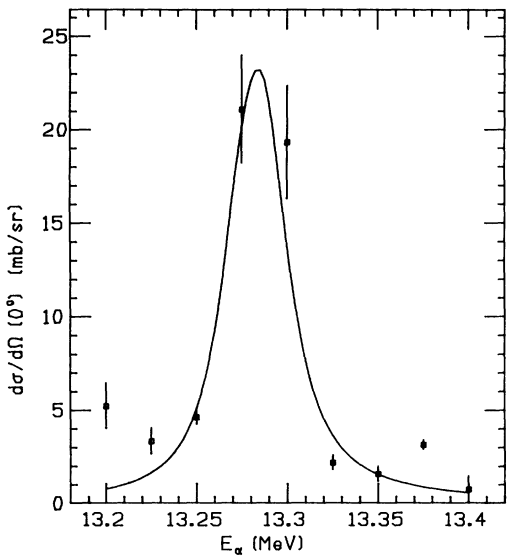

FIG. 10. The $l_{max}=6$ cross section around $E_\alpha=13.3$ MeV. The solid curve is a single-level R-matrix fit as discussed in the text.

At $E_\alpha=13.27$ MeV, corresponding to $E_x=15.34$ MeV in ^{20}Ne, the value of the single particle width for α decay to the first excited state in ^{16}O is $\Gamma_{s.p.}$(laboratory)=23.5 keV assuming a channel radius of 5.75 fm. From an analysis identical to that performed he $J^\pi=2^+$ level at $E_x=12.44$ MeV we find that the values for Γ_{α_1} can range from a small fraction of $\Gamma_{s.p.}$ to more than $\Gamma_{s.p.}$. A typical fit to the data is shown as a solid line in Fig. 10. Since there is no evidence for a strong $J^\pi=6^+$ level in the elastic data, we conclude that the state we are observing has a small elastic branching ratio. If we assume that the α_1 branching ratio for this level is at least as large as the α_0 branching ratio, we find $\Theta^2_{\alpha_1}>22\%$. Finally, we note that a value of 1 for $\Theta^2_{\alpha_1}$ would imply $\Gamma_{\alpha_1}/\Gamma=0.60$ and $\Gamma_{\alpha_0}/\Gamma=0.045$.

This 6^+ level, which may have a significant overlap with the [$\alpha+^{16}O(0_2^+)$] channel, may be contrasted with the $E_x=15.16$ MeV 6^+ level suggested by Hindi *et al.* to have similiar structure to the $E_x=12.44$ MeV 0^+ state. The 15.16 MeV 6^+ level and an 8^+ level at $E_x=18.54$ MeV were assigned [22,23] to a rotational band built on the $J^\pi=0^+$ level at $E_x=12.44$ MeV. This state was conjectured to be part of a band headed by the $E_x=12.44$ MeV level because of its small reduced width for α_0 decay and because of its large reduced width for α decay to the third excited state in ^{16}O ($J^\pi=2^+, E_x=6.92$ MeV) that belongs to a band headed by the first excited state in ^{16}O. The $J^\pi=8^+$ level was placed in the band primarily because of its large reduced width for decay via ^8Be emission. Because a large reduced width for α_1 decay is the distinguishing feature of both the $E_x=12.44$ MeV level and of the $E_x=13.1$ MeV level this property should be measured for the $E_x=15.16$ and 18.54 MeV states as well. The best previous estimate for the α_1 branching ratio for the $E_x=15.16$ MeV level is

$\Gamma_{\alpha_1}/\Gamma < 0.04$ which corresponds to $\Theta^2_{\alpha_1} < 0.2$ and was established [26] by Young *et al.* In the case of the $J^\pi = 8^+$ level, no α_1 branching ratio has been reported.

Because the α_1 branching ratio of the $J^\pi = 6^+$ level was already known to be small [26], we did not expect to observe it strongly in the $^{16}O(\alpha,\alpha_1)^{16}O$ reaction, and, in fact, neither it nor the 8^+ level was observed. Accordingly, we used the $^{12}C(^{12}C,\alpha)^{20}Ne^*$ reaction to study these levels. This eight-nucleon transfer reaction is known to populate both levels strongly and illustrates the additional kinematic freedom provided by three-body final state to study the continuum. We utilize this freedom by optimizing the bombarding energy to favor population of the state of interest relative to nearby states and the underlying background. For the $J^\pi = 6^+$ level, the beam energy was 36.3 MeV which is the energy used by both Young *et al.* [26] and Fifield *et al.* [24] in their angular correlation studies. In Fig. 11 we present (a) a singles spectrum, (b) the same spectrum in coincidence with a NaI detector with gates set to include high-energy gamma rays from decays of excited states in ^{16}O, and (c) in coincidence with the electron detector. The 15.16 MeV level is strong in singles relative to the background. It appears strongly in coincidence with gamma rays but only very weakly in coincidence with the electron detector. In this figure and in Fig. 12 the apparent discontinuities in the spectra are well understood artifacts of the position sensitive detector used in the focal plane of the spectrometer. The detector uses resistive charge division

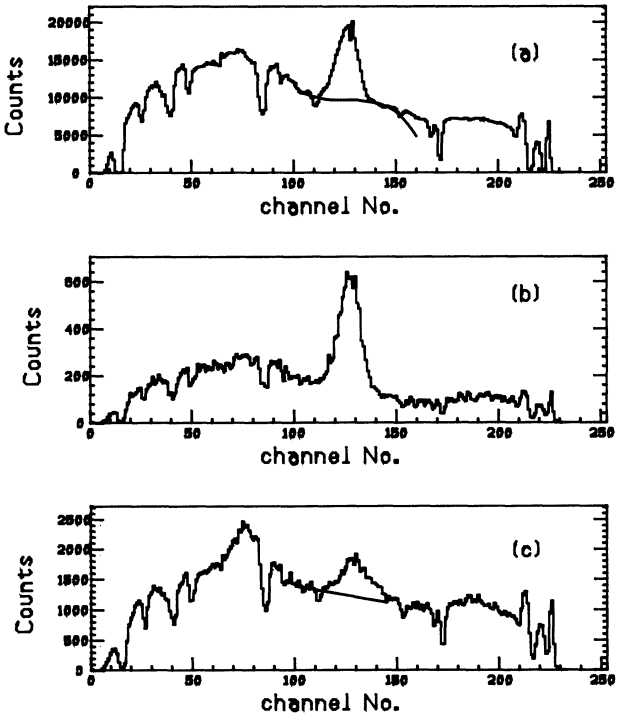

FIG. 11. Histograms from the branching ratio measurements for the $J^\pi = 6^+$ level at $E_x = 15.16$ MeV. (a) is a prescaled 0° α singles spectrum, (b) is in coincidence with γ rays, and (c) in coincidence with electrons or positrons.

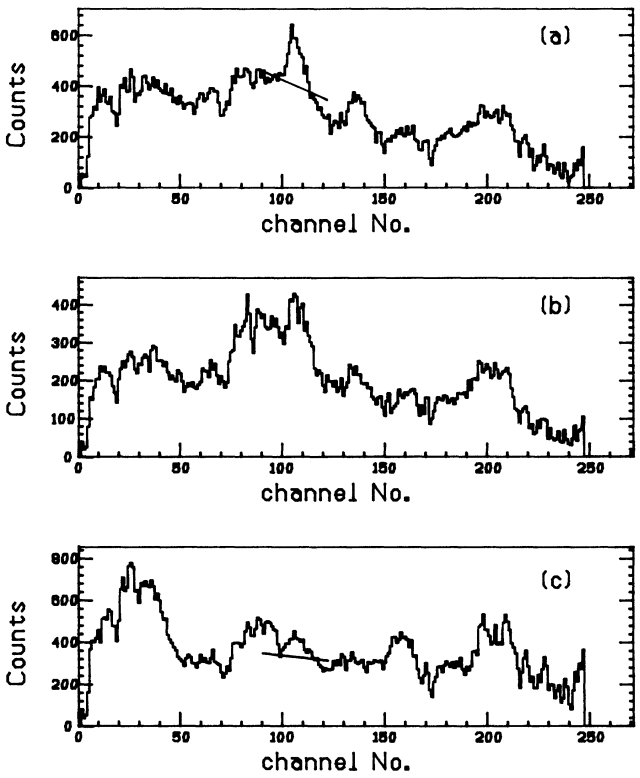

FIG. 12. Histograms from the branching ratio measurements for the $J^\pi = 8^+$ level at $E_x = 18.54$ MeV. (a) is a prescaled 0° α singles spectrum, (b) is in coincidence with γ rays, and (c) in coincidence with electrons or positrons.

for its position sensitivity and nonunformities in resistance cause the gaps.

The measurement of the decay of the $J^\pi = 8^+$ level at $E_x = 18.54$ MeV was made at a ^{12}C beam energy of 61 MeV which was the upper limit of our accelerator at the time of the experiment. Although this is somewhat below the beam energy of 64 MeV used in Refs. [22] and [23], we believe that we are producing the same state in ^{20}Ne. Our results for the 8^+ state are shown in Figs. 12, which is similiar to Fig. 11.

The α_1 branching ratio is given by

$$\frac{\Gamma_{\alpha_1}}{\Gamma} = \frac{N_c}{N_s \epsilon_e},$$

where N_c is the number of counts in the peak of interest in the electron coincidence spectrum and N_s is the corresponding number in the singles spectrum. ϵ_e is the electron detector efficiency for identifying decays passing through the first excited state in ^{16}O. In determining N_c and N_s, a background was subtracted as shown in Figs. 11 and 12. For the $J^\pi = 6^+$ level, we obtain a branching ratio of

$$\left.\frac{\Gamma_{\alpha_1}}{\Gamma}\right|_{\text{unc}} = (1.89 \pm 0.06) \times 10^{-2}$$

and for the $J^\pi = 8^+$ level we obtain

$$\left.\frac{\Gamma_{\alpha_1}}{\Gamma}\right|_{\text{unc}} = (1.76 \pm 0.22) \times 10^{-2}.$$

These values have not been corrected for counts that appear in the coincidence spectrum as a result of gamma rays which trigger the electron detector, e.g., by pair production in material in the vicinity of the target. It is important to consider the efficiency of the detector for photon events, ϵ_γ, because, as we have seen in Figs. 11 and 12 and by the above uncorrected branching ratios, decays of these ^{20}Ne levels to states in ^{16}O that produce photons are much stronger than those to the first excited state. Such a correction is difficult to make precisely because the mechanism by which a gamma ray can trigger the detector is not completely understood and depends in principle on the geometry of the scattering chamber and on the direction of emission of the photon [31].

In the present case we can justify using the value of ϵ_γ measured in a separate calibration experiment. Efficiency measurements for the detector were made immediately prior to the experiment using the reaction $^{16}O(p,p')^{16}$) as explained in Ref. [31]. The proton beam energy was 8.9 MeV which excites a previously known $J^\pi = 5/2^-$ resonance. If we assume that the decay from the resonant level to the $J^\pi = 3^-$ state in ^{16}O is by s-wave proton emission, a reasonable assumption in view of the low available energy in the c.m. system, then we can calculate the magnetic substate population of the $J^\pi = 3^-$ level without approximation and, using the formalism [43] of Rose and Brink, for example, the angular distribution of the gamma rays from its subsequent decay. In Fig. 13 we show plots of the gamma-ray angular distribution for the $^{16}O(p,p')^{16}O(J^\pi = 3^-)$ calibration reaction and for gamma rays from the decay of ^{16}O final states resulting from α decays of the $J^\pi = 6^+$ and 8^+ levels in ^{20}Ne. These later angular distributions were calculated by assuming that the $6^+ \rightarrow 3^-$, $8^+ \rightarrow 3^-$, etc., α decays are dominated by the lowest allowed angular momentum since this angular momentum is strongly favored by the exit channel penetrabilities.

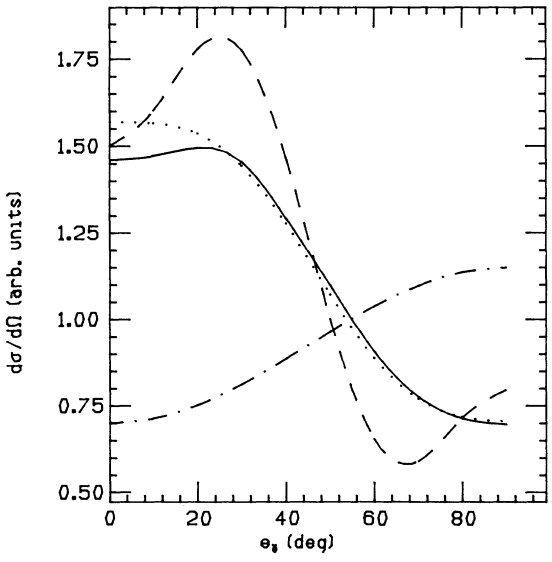

FIG. 13. Comparison of γ-ray angular distributions from the decay of the final ^{16}O states as populated in the ^{20}Ne, $E_x = 15.16$ MeV (solid line) and $E_x = 18.54$ MeV (dotted line) branching ratio measurement and in the γ efficiency measurement (dashed line). The dot-dashed line is the γ angular distribution from α_4 decays of the $E_x = 18.54$ MeV level.

The calculated angular distribution for gamma rays from the decay of the $J^\pi = 6^+$ level was produced by calculating the angular distribution for α decays that leave ^{16}O in its $J^\pi = 3^-$ state and for decays that leave ^{16}O in its $J^\pi = 2^+$ state. These distributions were averaged together; the work [26] of Young *et al.* shows that branching ratios to these two states in ^{16}O are nearly equal and that decays to other γ-producing states are weak.

The angular distribution due to the decay of the $J^\pi = 8^+$ level was generated in a similiar manner by calculating angular distributions resulting from decays to second and third excited states in ^{16}O and weighting these with the branching ratios of Ref. [23]. As in the case of the $J^\pi = 6^+$ level, the γ-ray angular distributions for the calibration and for the branching ratio measurement are similar. Alpha decays to the third and fourth excited states in ^{16}O were unresolved in the work of Hindi *et al.*. We have assumed, as did the authors of Ref. [23], that all these decays go to the third excited state. If there were a large α_4 branch for the $J^\pi = 8^+$ ^{20}Ne level, the shape of the γ angular distribution could be affected significantly. This is illustrated by the plot of the γ angular distribution expected for such a branch.

For both ^{20}Ne levels the angular distributions are similar enough to that of the efficiency measurement that we can use the measured value of ϵ_γ to make a correction to the α_1 branching ratio for the gamma ray efficiency of the electron detector. Our corrected α_1 branching ratio for the $J^\pi = 6^+$ level is

$$\frac{\Gamma_{\alpha_1}}{\Gamma} = 0.0099 \pm 0.0032 .$$

This corresponds to a reduced width of

$$\Theta^2_{\alpha_1} = 0.045 \pm 0.018 .$$

The quoted error is dominated by the error arising from the subtraction of the gamma-ray contribution to the branching ratio. This includes a 25% statistical uncertainty in the measurement of ϵ_γ in quadrature with an additional 25% uncertainty that was assigned to account for possible differences in the angular distribution of gamma rays between the $^{16}O(p,p')^{16}O$ calibration and the $^{12}C(^{12}C,\alpha)^{20}Ne^*$ reaction. There is a 25% uncertainty in the value of the reported total width, Γ, of the $J^\pi = 6^+$ level that contributes to the error assigned to the reduced width but not to the branching ratio. The value of the corrected α_1 branching ratio for the $J^\pi = 8^+$ level is

$$\frac{\Gamma_{\alpha_1}}{\Gamma} = 0.0097 \pm 0.0037$$

and corresponds to a reduced width of

$$\Theta^2_{\alpha_1} = 0.034 \pm 0.013 ,$$

with uncertainties calculated in the same way as for the 6^+ state

The reduced widths in the α_1 channel for both levels are of the order of a few percent. This is characteristic for decays between states with no particular structural relationship; for example, the 13.1 MeV 2^+ state has a similiar reduced width in the α_0 channel. We conclude that neither the $J^\pi=6^+$ nor 8^+ levels in ^{20}Ne which were assigned [22,23] to a band headed by the $J^\pi=0^+$ level at $E_x=12.44$ MeV exhibit the most salient feature (a large value of $\Theta^2_{\alpha_1}$) of the $J^\pi=0^+$ level and the $J^\pi=2^+$ level at $E_x=13.1$ MeV.

IV. CONCLUSIONS AND DISCUSSION

In these experiments we have examined the α_1 decay channel of quasi-bound levels in ^{20}Ne. A primary goal is to identify levels in ^{20}Ne which are structurally related to the $J^\pi=0^+$ level at $E_x=12.44$ MeV. In this section we discuss the predictions of the nuclear shell model, and of the cluster model of Wildermuth and McClure [44] and compare them with our results. A frequently used concept is that of the rotational band. This term is usually used to mean a set of nuclear levels that are structurally related and, as a consequence, share some common features such as modes of decay. Levels in a band are generally strongly connected by electromagnetic $E2$ matrix elements and often exhibit a characteristic energy spacing proportional to $J(J+1)$, where J is the nuclear angular momentum quantum number. The assignment of a nuclear level to a particular rotational band implies that no other state of the same spin can be constructed within the model space that is as closely related to the other band members. In a cluster model such as the one described by Wildermuth and McClure [44] the wave function of the nucleus is written as the antisymmetrized product of intrinsic clusters and a relative wave function. Levels belonging to the same band all have identical intrinsic cluster wave functions and the relative wave functions all have the same number of oscillator quanta but differ only in the orbital angular momentum quantum number l.

As an example of the kinds of values one can get for α particle reduced widths from the shell model, we note that Ichimura *et al.* [45] calculated $\Theta^2_{\alpha_0}$ for decays from the ground-state band in ^{20}Ne to the ground state of ^{16}O. The ^{20}Ne wave functions were taken to be four particles in the $2s$-$1d$ shell coupled to a closed ^{16}O core so the calculated quantites are typical "large" values for shell-model α reduced widths. Using the wave functions of Akiyama, Arima, and Kubo [3], Ichimura found $\Theta^2_{\alpha_0}$ to be very nearly 20% for all levels in the band and from 12% to 19% when he used the wave functions of McGrory [45].

Brown [21] calculated shell-model $J^\pi=0^+$ wave functions for ^{20}Ne and ^{16}O in which he assumed a closed ^{12}C core and active $1p_{1/2}$, $1d_{5/2}$, and $2s_{1/2}$ orbitals. Although his calculation produced several ^{20}Ne levels near 12.44 MeV, it generated no levels above an excitation energy of 8.5 MeV with values for $\Theta^2_{\alpha_1}$ greater than 4%. The inability of the calculation to reproduce the properties of the observed level could possibly be a result of the restricted model space, e.g., the neglect of the $1d_{3/2}$ orbital.

The present results also shed some light on a possible description of these core-excited levels in ^{20}Ne in terms of the weak-coupling model. The idea here is to represent an 8p-4h state by a product wave function in which the 8 particles occupy the same *sd*-shell orbits as identifiable low-lying states of ^{24}Mg; correspondingly the 4 holes represent low-lying states of ^{12}C. This ansatz gives a reasonably successful description of the previously known 8p-4h states [15,16] in the band built on the 0^+_3 state in ^{20}Ne. In this case the band head is based on the g.s. of ^{24}Mg coupled to the g.s. of ^{12}C. In the case of a possible band built on the $J^\pi=0^+$, $E_x=12.44$ MeV level, a possible candidate configuration is ^{24}Mg ($J^\pi=0^+$, $E_x=6.44$ MeV) $\otimes$ ^{12}C(0^+, g.s.), with a possible admixture of ^{24}Mg(0^+, g.s.) $\otimes$ ^{12}C($J^\pi=0^+$, $E_x=7.6$ MeV). In addition to the approximately correct differences in excitation energies (the 12.44 MeV state is approximately 5 MeV above the 8p-4h 0^+_3 state in ^{20}Ne), the 0^+_2 state in ^{24}Mg is known to have a relatively large spectroscopic factor for α transfer [46]. In this simple model the four-particle overlap between ^{20}Ne($E_x=12.44$ MeV) and ^{16}O(0^+_2) is the same as that between the ^{24}Mg(0^+_2) and ^{20}Ne(g.s.), because in the weak-coupling picture the ^{16}O (0^+_2) state has the configuration ^{20}Ne(g.s.) $\otimes$ ^{12}C(g.s.). The present results do not appear to support this simple interpretation, which would require that the 2^+ member of the band (assigned in the present study as the $E_x=13.1$ MeV $J^\pi=2^+$ state) have the configuration ^{24}Mg(2^+_3) $\otimes$ ^{12}C(0^+, g.s.) + ^{24}Mg(0^+_2) $\otimes$ ^{12}C(2^+). Naively, if the first configuration is dominant, one would expect a large spectroscopic factor for α transfer for the corresponding 2^+ state in ^{24}Mg. In fact, the α-particle spectroscopic factors for the 0^+ and 2^+ members of the 0^+_2 band in ^{24}Mg are not approximately equal; rather, the measured ratio is $S_\alpha(2^+)/S_\alpha(0^+)\approx 0.096$ [46]. It is of course possible that the observed results could be reproduced by a more complicated weak-coupling picture in which the two configurations (involving excitations of the 8 particles or the 4 holes) interfere, but the presently available evidence is insufficient to provide a definitive test.

Since it is difficult to reproduce values as large as we have measured for α-particle reduced widths within the context of the shell model, we should ask if other models, those which emphasize collective degrees of freedom, can do better. The cluster model of Wildermuth and McClure [44] was introduced as a variational method to provide a set of basis states for calculations of nuclear quantities. The hope is that by exploiting the saturation of the nuclear force and the large binding energies of particular structures such as α particles one can intuitively choose trial wave functions that are close to the physical eigenfunctions. Cluster models are a natural way to think about states with large α decays because we can treat the compound nucleus as an antisymmetrized product of an α particle and a residual (^{16}O) nucleus.

There is no advantage to using the cluster model over

the shell model unless we take advantage of the cluster model's ability to exploit nuclear correlations that are likely to exist in the system under study. This can be done by introducing parameters into the wave function which are believed physically meaningful. In a full calculation, the best values for the parameters are often found by minimizing the energy expectation values of the trial wave functions subject to orthogonality and normalization constraints. In the present case, one would wish to modify the cluster wave function in a way that will produce larger values for the spectroscopic amplitudes. To do this we need to reduce the overlap of terms in the cluster model wave functions in which nucleons are exchanged between the two clusters. These exchange terms arise from antisymmetrization between the clusters. The most straightforward way of achieving this goal is to modify the relative wave function so that its value at distances comparable to or smaller than the mean cluster radius is small compared to its value at larger distances (i.e., we need to keep the clusters apart). A consequence of this modification is that there no longer exists a trivial equivalence between the cluster and shell models.

We summarize some of the major results of our experiments in Table I. The $J^\pi=0^+$ and 2^+ levels at ^{20}Ne excitation energies of 12.44 and 13.1 MeV, respectively, are quite similar in that they both appear as isolated levels in the $^{16}O(\alpha,\alpha_1)^{16}O$ reaction and they both have exceptionally large reduced widths for α decay to the first excited state in ^{16}O. We conclude that both of these levels are structurally related and that they are most naturally interpreted in terms of a model that allows more collectivity than that found in single-particle models. Since both of these states have extreme values for their reduced widths for α_1 decay, they should be thought of as an α particle coupled to the first excited state of ^{16}O by an elongated relative wave function. The picture of two subsystems coupled to each other by a wave function that is stretched out enough that antisymmetrization effects are diminished is reminiscent of a molecule, and much work has been done on the development of nuclear molecular models (e.g., Refs. [15, 47–57]).

We conclude that the $J^\pi=2^+$ level at $E_x=13.1$ MeV belongs in a band with the $J^\pi=0^+$ level at $E_x=12.44$ MeV since these two states share the same, unusual decay mode. We disagree with the suggestion of Hindi *et al.* that the $J^\pi=6^+$ and 8^+ levels at $E_x=15.16$ and 18.54 MeV are also members of this band for this would imply that these $J^\pi=6^+$ and 8^+ levels are more closely related to the $J^\pi=0^+$ and 2^+ states than are any other possible states of spin 6 or 8. We have seen that, in view of their large values of $\Theta^2_{\alpha_1}$, a natural interpretation of $J^\pi=0^+$ and 2^+ levels is in terms of a cluster model in which an ^{16}O in its first excited state is coupled to an α particle. In this model, higher-spin states belonging to the same band (i.e., states which are as closely related as possible) would also have large values of $\Theta^2_{\alpha_1}$, in contrast to the behavior observed for these $J^\pi=6^+$ and 8^+ levels.

In the $^{16}O(\alpha,\alpha_1)^{16}O$ experiment we found candidates for other members of a rotational band whose head is the $J^\pi=0^+$ level at $E_x=12.44$ MeV. It is likely that a $J^\pi=4^+$ level with large reduced width for α decay to the first excited state in ^{16}O is in the region between $E_\alpha=11.2$ and 12.7 MeV that we analyzed in detail. Every fit [35], with one exception, with the effective $l=4$ cross section contains an individual level with a value of $\Theta^2_{\alpha_1}$ greater than 30%. In any event a large amount of strength for decay into the α_1 channel is concentrated in this energy range.

Our first inclination was that a $J^\pi=6^+$ level with a large value of $\Theta^2_{\alpha_1}$ might be somewhere in the $l=6$ structure evident between $E_\alpha=15$ and $E_\alpha=17.5$ MeV. However, the data do not appear to require this conclusion. In region A we have been able to fit the data with a set of level parameters in which the largest value of $\Theta^2_{\alpha_1}$ for an individual level is less than 5%. In region B every fit con-

TABLE I. Reduced widths for some continuum levels in ^{20}Ne.

J^π	E_x(MeV)	$\Theta^2_{\alpha_1}$	Notes
0^+	12.436±0.004	≈1.15	a
2^+	13.095±0.006	>0.63	
4^+	13.69−14.93	$\sum\Theta^2_{\alpha_1}>0.5$	b
6^+	16.73−18.73	$\sum\Theta^2_{\alpha_1}>0.3$	c
6^+	15.346±0.002		d
6^+	15.16	0.045±0.018	
8^+	18.54	0.034±0.013	

[a]Reference [21].
[b]Divided among 8 levels.
[c]Divided among 16 levels.
[d]See text.

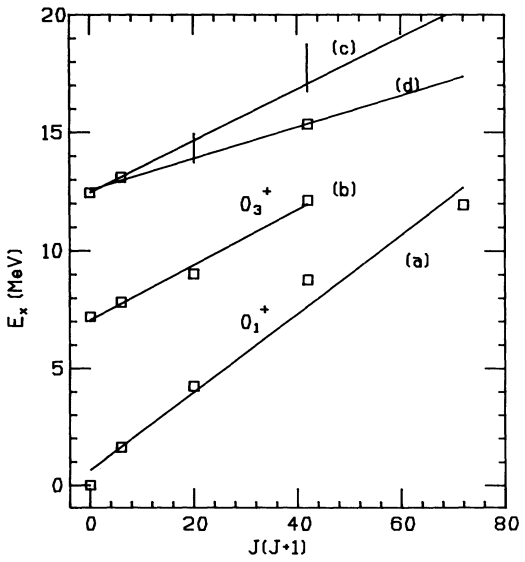

FIG. 14. (a) $K^\pi=0_1^+$ and (b) 0_3^+ bands in ^{20}Ne. The lines are linear fits to the points. Also shown are possible levels or regions of levels for a new $K^\pi=0^+$ band. Line (c) is a fit to the 0^+ and 2^+ levels. Line (d) is a fit to the 0^+, 2^+, and the single 6^+ level.

tains a level with at least a 14% reduced width. Although this is a moderate value for $\Theta^2_{\alpha_1}$, the data from which it was extracted are of poorer quality than in region A. The possibility also exists of substantial $l=6$ α_1 strength at lower excitation energy. In particular, the single state at $E_x = 15.34$ MeV could contain more spectroscopic strength in the α_1 channel than the region discussed above.

It is interesting to consider the energy dependence of the α_1 strength as a function of angular momentum within the context of the rotational model. Figure 14 shows the states (squares) or ranges of excitation energy (vertical lines) where we have identified substantial α_1 strength. Also shown, for purposes of comparison, are the previously known rotational bands built on the ground state (marked "a") and built on the 0^+_3 (believed to be predominantly 8p-4h in the structure marked "b"). It is immediately clear that *any* interpretation of the present data using the rotational model will require an extended structure with a large moment of inertia. To make this more quantitative, the curve labeled "c" in Fig. 14 is a straight line fitted to only the 0^+ and 2^+ states at $E_x = 12.44$ and 13.1 MeV; this line passes through the concentrations of 4^+ and 6^+ strength. The moment of inertia deduced from the slope of this curve is $4.55\ \hbar^2$ MeV^{-1}, quite similar to the value $4.28\hbar^2$ MeV^{-1} which characterizes the $K^\pi = 0^+_3$ band already believed (see Refs. [8–13]) to be dominated by 8p-4h configurations. Associating the 6^+ strength of the higher 8p-4h band with the single state at $E_x = 15.34$ MeV results in an even higher moment of inertia; curve "d" in Fig. 14 is a least squares fit to the 0^+, 2^+, and 6^+ states. The curve passes through the region of 4^+ strength and gives moment of inertia of $7.47\hbar^2$ MeV^{-1}. This would correspond to a structure even more extended in space that that based on the lower 8p-4h band. Distinguishing between these two possibilities is not possible with presently available data.

This fragmentation of the α_1 spectroscopic factor possibly starting in the $J^\pi=4^+$ region and increasing in the $J^\pi=6^+$ region suggests that at higher angular momenta the picture of a molecular resonance begins to break down and may be an indication that other dynamical degrees of freedom are becoming important. This is reasonable since the number of ways one can partition a nuclear system grows with the excitation energy. At an excitation energy of 17 MeV there is enough energy in the system to break the ^{20}Ne nucleus into two alpha particles and a ^{12}C nucleus and still have 5 MeV of excitation energy left over, about what is needed to excite states in ^{12}C.

ACKNOWLEDGMENTS

We would like to thank Dr. E. F. Garman, Dr. D. P. Bybell, Dr. T. Chapuran, Dr. A. H. Wuosmaa, Dr. S. F. Pate, Dr. M. G. Burlein, and Dr. J. Arrison, and R. N. Laymon for their assistance in carrying out the experiments described herein. The foil targets used in the experiments were fabricated by L. Csihas. This work has benefitted from discussions with Professor F. Ajzenberg-Selove and Professor H. T. Fortune and Dr. M. A. Carchidi and Dr. J. W. Sweet. This work was supported by the National Science Foundation.

[1] J. P. Elliot, Proc. R. Soc. London **245**, 128 (1958); M. Harvey, *Advances in Nuclear Physics*, edited by M. Baranger and E. Vogt (Plenum, New York, 1968), Vol. 1, p. 67.
[2] T. Suzuki, A. Arima, and K. Kubo, Nucl. Phys. **A288**, 493 (1977).
[3] Y. Akiyama, A. Arima, and T. Sebe, Nucl. Phys. **A138**, 273 (1969).
[4] Y. Horikawa, Prog. Theor. Phys. **47**, 867 (1972).
[5] E. V. Inopin, V. S. Kinchakov, V. K. Lukyanov, and Yu. S. Pol, Ann. Phys. (N.Y.) **118**, 307 (1979).
[6] H. Walliser, T. Fliessback, and Y. C. Tang, Nucl. Phys. **A437**, 367 (1985).
[7] A. Arima, V. Gillet, and J. Ginocchio, Phys. Rev. Lett. **25**, 1043 (1970).
[8] R. Middleton, J. D. Garrett, and H. T. Fortune, Phys. Rev. Lett. **27**, 950 (1971).
[9] R. Middleton, J. D. Garrett, H. T. Fortune, and R. R. Betts, J. Phys. C **6**, 39 (1971).
[10] L. R. Greenwood, R. E. Segel, K. Raghunathan, M. A. Lee, H. T. Fortune, and J. R. Erskine, Phys. Rev. C **12**, 156 (1975).
[11] K. Nagatani, M. J. Le Vine, T. A. Belote, and A. Arima, Phys. Rev. Lett. **27**, 1071 (1971).
[12] R. R. Betts, H. T. Fortune, and R. Middleton, Phys. Rev. C **11**, 19 (1975).
[13] M. E. Cobern, D. J. Pisano, and P. D. Parker, Phys. Rev. C **14**, 491 (1976).
[14] J. B. McGrory and B. H. Wildenthal, Phys. Rev. C **7**, 974 (1973).
[15] Y. Fujiwara, H. Horiuchi, K. Ikeda, M. Kamimura, K. Kato, Y. Suzuki, and E. Uegaki, Suppl. Prog. Theor. Phys. **68**, 29 (1980).
[16] H. T. Fortune, private communication, 1988.
[17] A. Arima and D. Strottman, Nucl. Phys. **A162**, 423 (1971).
[18] G. E. Brown and A. M. Green, Nucl. Phys. **75**, 401 (1966).
[19] B. Apagyi and G. Fai, J. Phys. G **3**, L163 (1977).
[20] D. P. Balamuth, K. C. Young, R. W. Zurmühle, L. K. Fifield, T. J. M. Symons, and K. W. Allen, Proceedings of the International Conference on Nuclear Structure, Tokyo, Japan, 1977 [J. Phys. Soc. Jpn. Suppl. **44**, 244 (1978)].
[21] E. F. Garman, L. K. Fifield, W. N. Catford, D. P. Balamuth, J. M. Lind, and R. W. Zurmühle, Nucl. Phys. **A372**, 194 (1981).
[22] M. M. Hindi, J. H. Thomas, D. C. Radford, and P. D. Parker, Phys. Lett. **99B**, 33 (1981).
[23] M. M. Hindi, J. H. Thomas, D. C. Radford, and P. D. Parker, Phys. Rev. C **27**, 2902 (1983).
[24] L. K. Fifield, R. W. Zurmühle, D. P. Balamuth, and J. W. Noé, Phys. Rev. C **8**, 2203 (1973).
[25] H. T. Richards, G. T. Caskey, J. H. Billen, S. R. Riedhauser, and D. J. Steck, Phys. Rev. C **29**, 2332 (1984).
[26] K. C. Young, R. W. Zurmühle, J. M. Lind, and D. P.

Balamuth, Nucl. Phys **A330**, 452 (1979).
[27] E. F. Garman, Ph.D. dissertation, Oxford University, 1980.
[28] Y. K. Lee, L. W. Mo, and C. S. Wu, Phys. Rev. Lett. **10**, 258 (1963).
[29] J. Kramp, D. Habs, R. Kroth, M. Music, J. Schirmer, and D. Schwalm, Nucl. Phys. **A474**, 412 (1987).
[30] F. Ajzenberg-Selove, Nucl. Phys. **A475**, 1 (1987).
[31] W. K. Wells, D. Cebra, and D. P. Balamuth, Nucl. Instrum. Methods **223**, 103 (1984).
[32] J. H. Billen, Phys. Rev. C **20**, 1648 (1979).
[33] S. R. Riedhauser, Phys. Rev. C **29**, 1961 (1984).
[34] G. Caskey, Phys. Rev. C **31**, 717 (1985). G. T. Caskey, Ph.D. dissertation, University of Wisconsin, 1983, available through University Microfilms International, Ann Arbor, MI.
[35] C. M. Laymon, Ph.D. dissertation, University of Pennsylvania, 1989, available through University Microfilms International, Ann Arbor, MI.
[36] P. H. Kutt and D. P. Balamuth, Comput. Phys. **3**, 52 (1989).
[37] Harald A. Enge, Rev. Scien. Instrum. **29**, 885 (1958).
[38] A. M. Lane and R. G. Thomas, Rev. Mod. Phys. **30**, 257 (1958).
[39] E. Barrelet, Nuovo Cimento **8A**, 331 (1972).
[40] A. de Bellefon and A. Berthon, Nucl. Phys. **B109**, 129 (1976).
[41] Z. Basrak and F. Auger, Nucl. Phys. **A441**, 150 (1985).
[42] S. R. Riedhauser, Ph.D. dissertation, University of Wisconsin, 1983, available through University Microfilms International, Ann Arbor, MI.
[43] H. J. Rose and D. M. Brink, Rev. Mod. Phys. **39**, 306 (1967).
[44] K. Wildermuth and W. McClure, in *Springer Tracts in Modern Physics*, edited by G. Hohler (Springer-Verlag, Berlin, 1966), Vol. 41.
[45] Munetake Ichimura, Akito Arima, E. C. Halbert, and Tokuo Terasawa, Nucl. Phys. **A204**, 225 (1973).
[46] N. Anantaraman, H. E. Gove, J. Toke, and J. P. Draayer, Nucl. Phys. **A279**, 474 (1977).
[47] *Clustering Aspects of Nuclear Structure and Nuclear Reactions,* Proceedings of the Third International Conference, Winnipeg, Canada, 1978, edited by W. T. H. Van Oers, J. P. Svenne, J. S. C. McKee, and W. R. Falk, AIP Conf. Proc. No. 47 (AIP, New York, 1978).
[48] A. Arima, H. Horiuchi, K. Kubodera, and N. Takigawa, Adv. Nucl. Phys. **5**, 345 (1972).
[49] R. A. Baldock, B. Buck, and J. A. Rubio, Nucl. Phys. **A426**, 222 (1984).
[50] R. A. Baldock and R. A. Stratton, J. Phys. G **11**, 515 (1985).
[51] R. A. Baldock and B. Buck, J. Phys. G **12**, L29 (1986).
[52] B. Buck, C. B. Dover, and J. P. Vary, Phys. Rev. C **11**, 1803 (1975).
[53] Y. Fujiwara, H. Horiuchi, and R. Tamagaki, Prog. Theor. Phys. **61**, 1629 (1979).
[54] Y. Fujiwara, Prog. Theor. Phys. **62**, 122 (1979).
[55] Y. Fujiwara, Prog. Theor. Phys. **62**, 138 (1979).
[56] Suppl. Prog. Theor. Phys. **68** (1980).
[57] T. Tomoda and A. Arima, Nucl. Phys. **A303**, 217 (1978).